

Forming Superhelix of Double Stranded DNA from Local Deformation

Heeyuen Koh^{a,*}, Jae Young Lee^b, Jae Gyung Lee^c

^aSoft Foundry Institute, Seoul National University, 1 Gwanak-ro, Gwanak-gu, Seoul, 08826, Korea

^bDepartment of Mechanical Engineering, Ajou University, 206 World cup-ro, Yengtong-gu, Suwon, Gyeonggi-do, 16499, Korea

^cDepartment of Mechanical and Aerospace Engineering, Seoul National University, 1 Gwanak-ro, Gwanak-gu, Seoul, 08826, Korea

Abstract

The forming 1.7 turn of the superhelix of DNA strands is the quintessential step of DNA packaging. However, the sequence dependent nonlinear elasticity of the molecule that causes nonlocal bend twist coupling makes the mechanism to form superhelix remain elusive. In this paper, the base pair wise geometrical constraints of the curved DNA strand address the deformation energy during a superhelix formation around a simplified core structure. The quantization of the energy in base pair wise unit characterizes the bend-twist coupling deformation that guides the accessible path to the superhelix deformation that forms 1.7 turns. Coarse-grained molecular dynamic simulation validates the description of the curvature formation process, which overcomes its persistence length.

Keywords: Nonlinearity, Nonlocality, Non-reciprocity, Superhelix, DNA, Polymer chemistry, Nucleosomal DNA, Bend-twist coupling, Coarse-grained simulation

1. Introduction

Characterizing the mechanism of the curvature formation process of DNA strands out of sequence dependent energetics of the double helical structure is of great significance to specify the functionality of the densely packed DNA strands in gene expression and regulation. The energetics decided from the non-linear and non-local elasticity of the dsDNA strand[1, 2, 3, 4] is supposed to intertwine with the readiness to form the nucleosomal-like conformation of the DNA strand[5], the 1.7 turn of superhelix. Yet, akin to many physical attributes tied to the curvature formation of superhelices, a complete framework for a precise understanding of the free energy affinity mechanisms in the superhelical formation of double-stranded DNA remains elusive.

The interaction between the strand and proteins[6, 7, 8] as the activation models of the superhelix formation process is another feature that challenges the theoretical description for the nonlocal elasticity of the strand due to the protein attachment that is locally defined on the strand.

*Corresponding author

Email address: heeyuen.koh@gmail.com (Heeyuen Koh)

The interaction with charged proteins[6, 7, 8] has been suggested beyond the scope that the current deformation model for double helical structure can reach since it presumes a strong bending of DNA strand from the separation of double strand as kinking[9, 10, 11], and such localized deformation has not linked to further curvature formation process for superhelix. Together with sequence-dependent elasticity[12, 13, 14] and the affinity of forming superhelix that is correlated with the persistence length of the strand[15] and the ion concentration[16], the initiation of curvature formation from localized deformation that starts 1.7 turns of superhelix has been the target that the theoretical frameworks of the curvature forming process of the double helical structure is required to explain for the energetic aspects associated with the free energy affinities of nucleosomal DNA configurations.

In identifying the physical properties related to curvature formation that completes 1.7 turns of superhelix, the geometrical condition in the wrapping process has distinctive attributes to the free energy landscape. The geometrical constraints of double helical structure related to how each base pair reacts to the curvature formation can offer the quantification of the free energy in detail based on recent nonlinear and nonlocal elastic models[3, 4, 2]. The result of the trial also provides the possible analysis of the free energy associated with the activation and curvature formation process of the nucleosomal DNA in a quantitative manner, including the effect of the anisotropic bendability caused by the proximity of the charged proteins[17] or ions.

The superhelix of the DNA strand has substantial twist deformation over 40 degrees with a radius of curvature of 5 nm as confirmed from the experiment[18] and all atom simulations[19]. Such geometrical preference has been presumed to be situated from continuing the curvature formation process to complete 1.7 turns of wrapping from localized deformation [20]. In this paper, we describe the deformation of curved DNA strands for each base pair with 3DNA variables using the framework for the double helical strand defined by Marko and Siggia[21] that is adapted with further details. Theoretical modeling is introduced in Section 2. The 1.7 turns of the superhelix and its formation process are explained using the geometrical modeling in Section 3. The paper is concluded in Section 4.

2. Geometry of the base pair in the curved double helical strand

2.1. Cartesian coordinates in curved strand

The local unit vectors defined for each base pair in the curved DNA strand with the geometry of the major-minor groove[21] describe various conformations heavily influenced by bend-twist couplings such as loop[22, 5, 12, 13] and plectonemes[1] with the following description:

$$\frac{d\hat{\mathbf{e}}_i}{ds} = (\vec{\Omega} + \omega_0\hat{\mathbf{e}}_3) \times \hat{\mathbf{e}}_i. \quad (1)$$

$\hat{\mathbf{e}}_i, i = 1, \dots, 3$ are the unit vectors of the coordinate system $\{\hat{\mathbf{e}}_i\}_{R0}$ on the cross section defined for a base pair. $\hat{\mathbf{e}}_1$ are aligned to make a two fold symmetry of the major-minor groove, and $\hat{\mathbf{e}}_3$ is along the normal vector at the center of the cross section. $\vec{\Omega}$ represents the rotation vector defined at s which is the arclength of the strand that has $\hat{\mathbf{e}}_3$ for its tangent. While Ω_1 and Ω_2 correspond to bending, Ω_3 describes torsion in $\vec{\Omega} = \Omega_1\hat{\mathbf{e}}_1 + \Omega_2\hat{\mathbf{e}}_2 + \Omega_3\hat{\mathbf{e}}_3$. ω_0 is the helicity of the strand which can be altered with additional twist deformation.

i th base pair on the strand arranged with the rotation vector $\vec{\Omega}(s_i)$ $i = 1, \dots, N$ with total number of base pairs in the strand, N in a curvature of the strand $\Omega^s(s)$. s_i is the location of

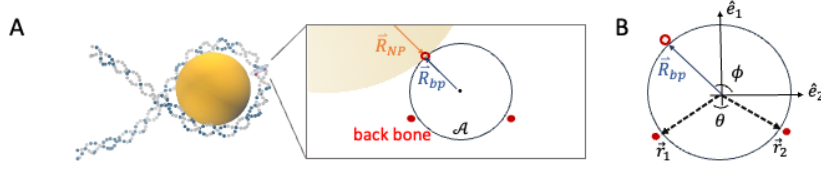


Figure 1: A. Schematic figure of a base pair in the superhelix curvature. \vec{R}_{NP} and \vec{R}_{bp} are the radius of NP and the cross section of base pair, \mathcal{A} . B. The unit vector of Cartesian coordinates defined on the cross section \mathcal{A} . Red hollow indicate the contact point between the cross section \mathcal{A} and NP. A yellow shadow indicates the existence of NP. Two red dots are the location of the nucleotides, and a hollow red circle indicates the contact point between the simplified core structure and cross section disk of a base pair.

i th base pair on the arclength of the strand. $\Omega^s(s)$ implies a line that is collected by \hat{e}_3 at every base pair in the strand. Because of the sequence dependent nonlocal and nonlinear elastic property of the DNA strand that affects bend-twist coupling, the rotation vector $\vec{\Omega}(s_i)$ is not decided by the curvature of the strand $\Omega^s(s_i)$. In this paper, the geometrically given deformation as unaffected by sequence dependent elasticity is separately noted with $\vec{\Omega}_{bp}$ distinguishing from $\vec{\Omega}(s_i)$. The details of how this geometrically given deformation results in superhelix formation with sequence dependent characteristics of the strand are dealt with in Section 3.

2.2. Geometrically given base pair wise deformation

When two nucleotides in a base pair lie along the vectors \vec{r}_1 and \vec{r}_2 respectively with the stacking vector \vec{l} between base pairs as shown in Fig. 1, the deformation of each nucleotide on the curvature of the strand, $\frac{d\vec{r}_j}{ds}$ with $j=1$ or 2 and the deformation on the stacking vector, $\frac{d\vec{l}}{ds}$ at the origin of the cross section of the base pair can be derived with $\frac{d\hat{e}}{ds}$ in Eq.(1) as followings:

$$\frac{d\vec{r}_j}{ds} = \frac{d}{ds} (r_{1j}\hat{e}_1 + r_{2j}\hat{e}_2) = r_{ij} \frac{d\hat{e}_i}{ds}, i, j = 1, \dots, 2, \quad (2)$$

$$\frac{d\vec{l}}{ds} = l \frac{d\hat{e}_3}{ds} = -l (\Omega_1 \hat{e}_2 - \Omega_2 \hat{e}_1). \quad (3)$$

r_{1j} and r_{2j} are the components of the vector \vec{r}_j , $j=1$ or 2 on the cross section \mathcal{A} . l is the stacking distance between base pairs.

The symmetry between two nucleotides determines the rotational deformation tilt(τ) and roll(ρ) in 3DNA variables[23, 24] from the derivation using the \hat{e}_3 component. The calculation for the deformation caused by the location of two nucleotides on the circumference of the base pair cross section \mathcal{A} noted with \vec{r}_j , $j=1$ or 2 is as follows:

$$\Delta = -\left(\frac{d\vec{r}_1}{ds} - \frac{d\vec{r}_2}{ds}\right) \cdot l_0 = \Delta_{\hat{e}_1} + \Delta_{\hat{e}_3}. \quad (4)$$

$$\Sigma = \left(\frac{d\vec{r}_1}{ds} + \frac{d\vec{r}_2}{ds}\right) \cdot l_0 = \Sigma_{\hat{e}_2} + \Sigma_{\hat{e}_3}. \quad (5)$$

$$\Delta l = l_0 \frac{d\vec{l}}{ds} = -l_0^2 (\Omega_1 \hat{e}_2 - \Omega_2 \hat{e}_1). \quad (6)$$

All equations above are derived from the approximation of the integration of Eq.(1) along the stacking distance between two base pairs. The stacking deformation Δl at the center of the cross section \mathcal{A} derived using Eq.(6) only has a lateral deformation along \hat{e}_1 and \hat{e}_2 . Therefore, the given theoretical derivations in this paper do not have the deformation on rise(D_z). This result justifies the usage of l_0 , which is the undeformed stacking distance between base pairs for the approximation of integral in Eq.(4)~Eq.(6). Eq.(6) has the square of l_0 from the differential term and the approximation in integration.

The direction of the deformation in subscript marks the deformation axis \hat{e}_i $i = 1, 2$ or 3 . $\Delta_{\hat{e}_3}$ and $\Sigma_{\hat{e}_3}$ imply the deformation of the nucleotides along \hat{e}_3 at the circumference of the cross section \mathcal{A} . Tilt(τ) makes the vector for each nucleotide in a base pair to have the opposite signs along the axis \hat{e}_3 so that the difference along \hat{e}_3 between the vector \vec{r}_1 and \vec{r}_2 becomes non zero. The negative sign in first equality in Eq.(5) compensates the calculation according to the definition of tilt(τ) which has plus sign of \hat{e}_3 on $r_{j2} > 0$ [23]. Roll(ρ) has the two nucleotides lifted along \hat{e}_3 on the circumference of the cross section simultaneously. $1/2\Delta_{\hat{e}_3}$ and $1/2\Sigma_{\hat{e}_3}$ becomes to the tilt(τ) and roll(ρ), respectively. $1/2$ are for adjusting the value in Eq.(4) and Eq.(5). $\Delta_{\hat{e}_1}$ and $\Sigma_{\hat{e}_2}$ are the translational displacements from a helicity of the strand and the twist(ω) deformation. The result of full derivation, including its quantification, is explained in the next subsection.

In the case of twist(ω), the two points corresponding to each nucleotide are shifted with the same angle on the circumference of the cross section \mathcal{A} , which means each point experiences the same amount of deformation along \hat{e}_1 and \hat{e}_2 at the same time. The twist(ω) deformation can be quantified from the minimum value between Ω_1 and Ω_2 in Eq.(6) because the common deformation between two nucleotides on the circumference of the cross section is equivalent to $\Delta\omega \hat{e}_3 \times \hat{e}_i = \Delta\omega (\hat{e}_2 - \hat{e}_1)$ for $i = 1, 2$ and 3 . $\Delta\omega$ is, then, $l_0^2 \Omega_1$ when $|\Omega_1| < |\Omega_2|$ and $\Omega_1 \cdot \Omega_2 > 0$. This twist deformation is not from an external source, and it is derived as the geometrical condition when the base pair experiences bending deformation along Ω^s . The deformation along the lateral direction along \hat{e}_1 and \hat{e}_2 at the center of the cross section \mathcal{A} becomes the bending component when the two components are not in phase to induce twist. Therefore, Δl in Eq.(6) also shows the possible source of stretch bending coupling when the radius of the cross section \mathcal{A} is not considered.

The rotational variables like tilt(τ), roll(ρ) and twist(ω), can be expressed in curvature unit, $\Omega_{bp} = (\Omega_\tau, \Omega_\rho, \Omega_\omega)$ for each variable is the segment of circumference that is drawn from the rotation along each axis of \hat{e}_{R0} . Note that Ω_{bp} is the result of derivation from $\Omega^s(s_i)$. The geometrically determined Ω_{bp} at s_i should be modified accordingly with the elasticity characteristics of the strand which has sequence dependent, nonlinear and non local conditions in the interaction with histone protein to be a nucleosomal DNA. The scope of the paper is restricted to consider geometrically given deformation to avoid further complexities.

The result from Eq.(4)~Eq.(6) also offers the information on the translation deformation.

Rise(D_z) is zero as mentioned in the previous paragraph, the \hat{e}_2 component Eq.(4) becomes Slide(D_y) which is $1/2\Sigma_{\hat{e}_2} + l_0^2\Omega_1$, and \hat{e}_1 component $-l_0^2\Omega_2$ in Eq.(5) is equivalent to Shift(D_x). Additionally, we should notice that the result of the deformation of stacking vector \vec{l} in Eq.(6) is equivalent to stretch-bending coupling condition, which is "non-reciprocal" because the lateral deformation along \hat{e}_1 and \hat{e}_2 at the center of the cross section \mathcal{A} does not offer any possible stretch.

2.3. Quantification of base pair wise deformation

A superhelix of nucleosomal DNA is built with multiple protein attachments at different regions simultaneously[20]. We presume that a spherical core structure like a nanoparticle can start the curvature formation for superhelix on one of such regions of the strand. The quantification for the series of multiple attachments of the proteins is not considered in this paper. The curvature Ω^s is, then, supposed to be around the artificially given spherical nanoparticle(NP) as forming a superhelix. Even though a spherical bead is the hypothetical core structure, this simplification has been utilized to study the superhelix or curvature formation of dsDNA strands with the attachment of ions and proteins. Few simulation studies[15, 16] alongside the experiment using the bare gold nanoparticles with long DNA strands[25] also prove the possibility of the excessive curvature formation wrapping of the nanoparticle.

The quantification of the given deformation derived by the geometry of double helix is investigated when the curvature Ω^s draws an ideal superhelix as the nucleosomal DNA with a few more assumptions like 1)the contact with NP does not cause torsional deformation directly, 2)the derivation does not include the effect of groove deformation and 3)there is also negligible radial deformation of the cross section of the base pairs and its stacking distance. Based on these assumptions, the derivation is restricted to evaluate the base pair wise deformation variables commonly presumed to be the main deformation source of dsDNA strand[23]. Further resolution of deformation between nucleotides, such as buckling, propeller, or opening variables, are not considered.

During the curvature formation around the core structure, which is modeled as NP, the strand curved on the surface of NP, as shown in Fig. 1A has a rotation of the cross section \mathcal{A} along the normal vector \hat{e}_3 to form the curved strand. The hollow circle in Fig. 1A becomes a rotation center of the cross section \mathcal{A} . The curvature drawing the strand along the NP surface makes the curvature of the strand Ω^s equivalent to the inverse of $|\vec{R}_{NP} - \vec{R}_{bp}|$. Here, \vec{R}_{NP} and \vec{R}_{bp} are the vector drawn from the center of the NP and that of the cross section \mathcal{A} to the contact point. If not, the strand would have either a curvature that is smaller than that of the surface of the NP so that the shape of the strand becomes partially attached to the surface of the NP or is attached as the multiple serpentine arclength on the surface of the NP with larger curvature than that of NP surface. The rotational vector in Eq.(1), $\vec{\Omega}$ in Eq.(1) is supposed to have the bending components whose norm is equivalent to the curvature of the strand, Ω^s .

The norm of the bending component of $\vec{\Omega}_{bp}$, therefore, becomes equivalent to that of Ω^s during the wrapping process around NP. The location of the rotation center, as shown in the schematic cartoons in Fig. 1B shows that the angle ϕ decides the bending component of $\vec{\Omega}_{bp}$, more specifically the ratio of Ω_1 and Ω_2 of $\vec{\Omega}$ defined by the Cartesian coordinate system of each base pair of the strand, which is derived in Appendix A. According to further derivation of Eq.(4)~Eq.(6 in Appendix B with the contact angle ϕ , Ω_1 and Ω_2 are directly proportional to roll(ρ) and tilt (τ), respectively as derived in Appendix B. Since the contact angle ϕ is shifted with 32.4° along the strand, the ratio of roll(ρ) and tilt (τ) also altered in neighbored base pairs

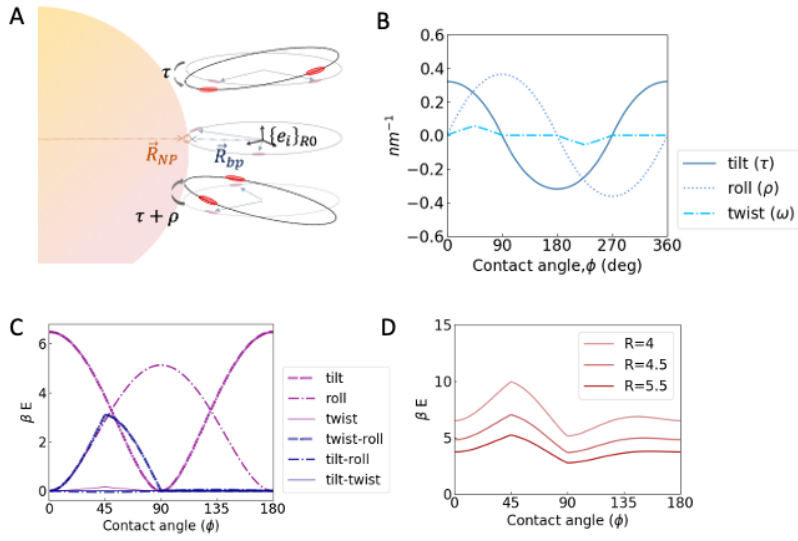


Figure 2: A. Schematic figure of roll(ρ) and tilt(τ) combination along the strand for its helicity on the surface of the NP (yellow shade), B. Deformation of each rotational variable in curvature unit along the contact angle, C. Deformation energy caused by each rotational variable and coupling condition calculated based on Eq. (C.1) based on the deformation curvature in B when the core structure has 7 nm diameter, D. Total deformation energy for a base pair to from the curvature around the NP with the radius 4 nm, 4.5 nm and 5 nm.

accordingly for the ratio of Ω_1 and Ω_2 is dependent on ϕ as shown in Fig. 2A. The twist deformation prompted by bending as $\Omega_3\hat{e}_3$ in $\vec{\Omega}_{bp}$ as given by Eq.(6) becomes by-products of bending curvature. The twist(ω) deformation is, therefore, solely dependent on the norm from Ω^s and the contact angle ϕ that decides the ratio between Ω_1 and Ω_2 . Therefore, the result of roll(ρ), tilt(τ), and twist(ω) from Eq.(4)~Eq.(6) is equivalent to the function of ϕ in the range of 0° to 360° as shown in Fig. 2B. The value of deformation is converted into curvature units to count the deformation energy. Additional details for the quantification are in Appendix B.

Each rotational deformation can be quantified along the location of the contact point from additional twist(ω) deformation in Fig. 2B and sequence dependent coupling rigidity. However, the interaction caused by the twist(ω) deformation to roll(ρ) or tilt(τ) is not included in the results in Fig. 2B for the amount of additional twist should be finalized by the sequence dependent coupling rigidity. The deformation energy along each type of deformation variables and their coupled condition is calculated from sequence averaged elasticity as shown in Fig.2C. Tilt(τ) and roll(ρ) deformation have the most intensified deformation energy level while the twist-roll($\omega - \rho$) coupling condition occupies a significant level of deformation energy. The detail is derived in Appendix C. The radius of curvature affects the general amount of deformation energy, as shown in Fig. 2D. Larger radius of curvature has less deformation energy since it is closer to the straight condition.

3. Superhelix formation

3.1. Spatiotemporal distribution

Further validation on Eq.(4)~Eq.(6) is conducted using the oxDNA1 and oxDNA2 simulation to confirm the geometric constraints derived from the major-minor groove, which is well dictated in oxDNA2 only. The thermostat derived from the heat diffusion process is adapted to oxDNA/oxDNA2 in the Lammmps package[26] since it is the only case that holds the stable wrapping conformation during 6 ns. Further details on the simulation result are in Appendix D. The conformation calculated by the Langevin thermostat shows identical wrapping conformation. Yet, the stability of the superhelix does not reach enough length to be analyzed. Additionally, the new thermostat[27] in oxDNA2 allows expansion of the scope of CG simulation with various conformations such as inch-worm translocation of the core structure[28] and the simultaneous wrapping conformation of two NPs. Animated gifs are included in the Supplementary Videos, and the persistence length measured with the new thermostat compared to the Langevin thermostat in Supplementary material.

All five distinguishable sequence strands are compared based on the results from the oxDNA2 simulation with the heat diffusion thermostat. Two sets of strands have shared the same sequence with small segments with different conditions to investigate the sequence dependent affinity. IAT strand has AGT sequence instead of AAT in the EXAT, so as c2 and c3 strands compared to c1 whose number of TA sequence occurrences increases in the order of $c2 > c3 > c1$. Among those, the contact angle(ϕ) for each base pair of c1 sequence calculated using oxDNA2 with NP is in spatiotemporal distribution in Fig. 3A. The angle is measured when the strand is near the NP in 6 nm of radius from the center of mass of the NP. The patterns shown in the spatiotemporal distributions of all 3DNA variables is identified with the result of derivation of Eq.(4)~Eq.(6) in terms of contact angle ϕ which is supposed to repeat 0 to 360 degree pattern of Fig. 2B along the strand during superhelix formation. The spatiotemporal distribution of roll(ρ), tilt(τ) and twist(ω) shows a clear pattern of contact angle(ϕ) as shown in Fig. 3B unlike the translational

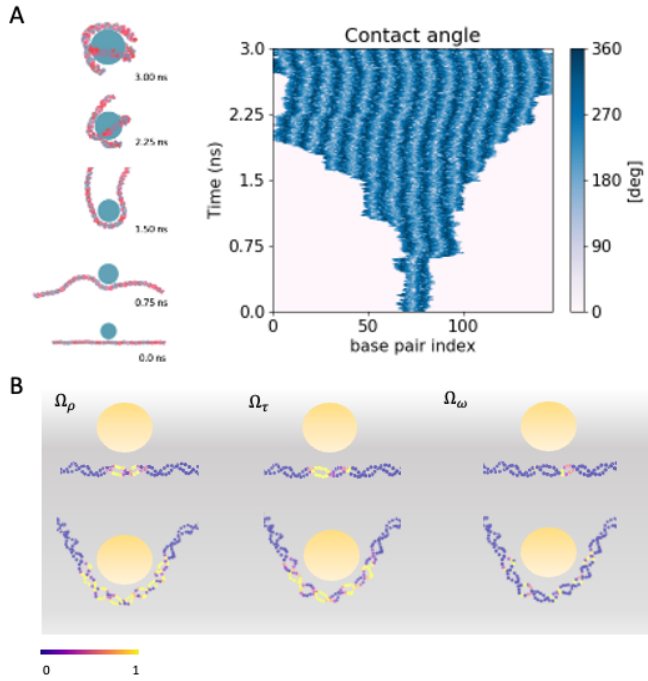


Figure 3: The angle between the contact point and the center of the base pair is measured as shown by spatiotemporal distribution. y axis is time, x axis is the index of base pair along the strands. The left inset is about the conformation change during the wrapping process of c1 strand. The angle and contact point are measured only when the distance from the center of NP to that of dsDNA is in 6 nm. B. Three rotational deformations along roll(ρ), tilt(τ) and twist(ω) in curvature unit on each base pair in the strand. Each deformation is normalized by its maximum value. Purple means zero deformation. Clear patterns in the approximately 11 base pair period are observed.

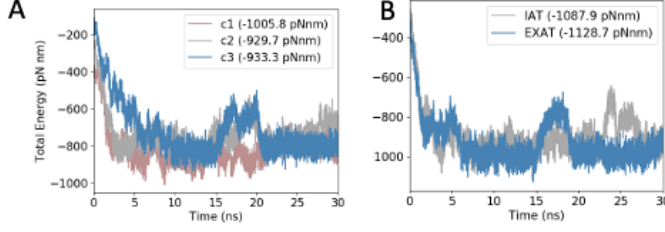


Figure 4: Total energy during wrapping process in 30 nm using oxDNA2 and new thermostat. A. c1 (pink) proves its minimum free energy level and rapid completion of wrapping. c2 and c3 strands have major re-arrangement of strands around the NP at 10 ~20 ns, which delays the completion. B. Total energy during the wrapping process. EXAT has a more stable condition than IAT according to the minimum energy (in parenthesis). The peak at 25 ns in IAT result bolsters the wrapping process of IAT completed slowly compared to EXAT.

deformation like $slide(D_y)$ and $rise(D_z)$ except $Shift(D_x)$ which well show the distribution as expected following the pattern of contact angle(ϕ). All strands have shown the repetition of the contact point angle(ϕ) ranging 0 to 360 in every 10.3 base pair period along the strand, as shown in Fig. 3B, which shows the normalized energy distribution along the strand during wrapping process around NP. In Fig 3B, The purple strand under deformation-free conditions changes its color along the strand as the curvature propagates around the NP in a yellow shade. All spatiotemporal distributions of three rotational variables and three translational variables along the strand during the wrapping formation of each strand are included in the Supplementary data. The information on the sequence of all five strands is also included in the Supplementary material.

The relative affinity calculated by Freeman et al.[14] for the wrapping process of each strand is measured without Thermodynamic Integration because the free energy level becomes accessible through the total energy[29, 30] in the oxDNA/oxDNA2 simulation which has a fine resolution of total energy owing to the heat diffusion damping process which minimizes the random distribution of thermal fluctuation. The Supplementary material and the URL in Acknowledgment include further details of the thermostat from the heat diffusion process. The results in Fig. 4A and B indicate that the sequence dependent preference followed by having less TA or AGT sequence in c1 and EXAT strands is beneficial in superhelix formation, respectively. Such preference of affinity marked in the legend of Fig. 4 is well presented as the duration of the wrapping process. c1 and EXAT have rapidly completed the conformation change while other cases prolonged more time than these two strand conditions. In the next subsection, we further excavate the wrapping path of the IAT and c2/c3 strands, whose curvature formation process is completed more slowly than the c1 and EXAT strands, as confirmed in Fig. 4A and B. The specific level of affinity and its calculation process are included in the Supplementary material.

3.2. Sequence dependent superhelix formation process

One of the features that oxDNA2 with new thermostat can distinguish between AAT and AGT for EXAT/IAT or TA replacement in c1/c2/c3 strands is the alternation of the sign of coupling rigidity between tilt(τ) and roll(ρ), $g_{\tau\rho}$. $g_{\tau\rho}$ has clear sequence dependent differences in the order of $O(10^{-2})$ in pN which is negligible in its energy contribution in Fig. 2C. The rigidity information that is measured using oxDNA2 with heat diffusion process, which is included in the

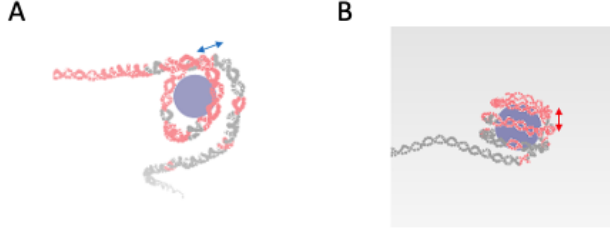


Figure 5: Wrapping using the CG model with major-minor groove(oxDNA2), B. Wrapping from CG model without major-minor groove(oxDNA). The distance between strands in wrapping conformation(red arrow) in the oxDNA case is narrower than that calculated using the oxDNA2 case(blue arrow).

Supplementary material confirms that its energy contribution is not significant compared to other conditions like the coupling between twist(ω) and roll(ρ), $g_{\omega\rho}$. However, $g_{\tau\rho}$ can regulate the speed and affinity of the wrapping process because the twist(ω) deformation of a base pair-wise cross section is decided from the specific combination of tile(τ) and roll(ρ), which is directly managed by the positive sign of $g_{\tau\rho}$ to have the opposite phase between Ω_1 and Ω_2 according to Eq.(6). The sign of each bending component is derived from the contact angle ϕ in the range of $[0^\circ, 90^\circ]$ and $[180^\circ, 270^\circ]$ as shown in Fig. 2B.

Note that the periodic structure of a double helix during 10.3 bp requires the full range of the contact points angle ϕ , which is $[0^\circ, 360^\circ]$. Therefore, the motive of deformation shown in Fig. 2B appears every 10.3 bps as demonstrated in Fig. 3B. Therefore, the twist(ω), which is defined as the phase between roll(ρ) and tilt(τ) should be shown twice repeatedly for every 10.3 bps to complete the curvature of superhelix. The long series of the negative coupling rigidity $g_{\tau\rho}$ alters the roll(ρ) or tilt(τ) deformation not to be in the phase with tilt(τ) or roll(ρ) so as hindering the twist(ω) formation.

The difference in affinity between c1/c2/c3 has a clear dependency on the number of appearances of the TA sequence since it has a negative value of $g_{\tau\rho}$. In case of c1/c2/c3, the prolonged time duration of the wrapping process of c2 and c3 becomes twice more extended than that of c1 in Fig. 4A. EXAT which has more number of the sequence with the positive sign of $g_{\tau\rho}$ becomes more stable than IAT according to the minimum free energy level of curvature formation as shown in Fig. 4B and the affinity measured by the energy difference between the bare strand and NP wrapping conformation as marked in the legend in Fig. 4B.

The consequence of pursuing the wrapping to be propagated along the strand with unresponsive $g_{\tau\rho}$ can make the shift of the contact angle of all base pairs attached to the NP and consequentially produces delays as shown in the range of 15 ns~20 ns for c2 and c3 strands in Fig. 4A and at 20 ns for IAT in Fig. 4B. Such delays can be confirmed from the spatiotemporal distributions in Supplementary material, which also shows the shifts in the pattern of contact angle with partial detachment of the strand from NP surface. The sequence dependent coupling rigidity for the IAT/EXAT is in the table in Appendix E. the c1/c2/c3 cases in Fig. E.7 shows the affinity of the wrapping conformation and the number of positive $g_{\tau\rho}$ in the c1/c2/c3 in a good agreement.

3.3. 1.7 turn superhelix induced by Major-minor groove

According to Eq.(4)~Eq.(6), the curved double stranded DNA experiences twist(ω) deformation induced from bending. From the quantification shown in Fig. 2B, the effect of this additional twist on translational deformation out of the plane of the curvature, the kurtosis, is analyzed. The kurtosis of the curved curvature is the deformation derived from shift(D_x) and slide(D_y) to be perpendicular to the plane where the curvature of the strand is defined. With additional twist(ω) deformation shown in Fig. 2B, each term of shift(D_x) and slide(D_y) which are $\vec{D}_x = l_0\Omega_2\hat{e}_1$ and $\vec{D}_y = r_{11}l_0(\omega_0 + \omega)\hat{e}_2 - l_0^2\Omega_1\hat{e}_2$, respectively, can be calculated with coordinate transformation along the new axis aligned along \vec{R} and the axis normal to the plane with curvature of the strand. The coordinate system for such kurtosis is defined by the coordinate translation with the angle ϕ as $\hat{e}_K = -\sin\phi\hat{e}_2 + \cos\phi\hat{e}_1$ which is derived in Appendix F. When additional twist deformation(ω) occurs from the bending, as derived by Eq.(6), the kurtosis can be specified. The quantification of the kurtosis, \mathcal{K} can be expressed in followings:

$$\begin{aligned}\mathcal{K} &= D_x \cos \phi - D_y \sin \phi \\ &= l_0^2\Omega_2 \cos \phi - (1/2\Sigma\hat{e}_2 + l_0^2\Omega_1) \sin \phi \\ &= -1/2\Sigma\hat{e}_2 \sin \phi \pm 2l_0^2\Omega \sin 2\phi \\ &= 1/2r_{11}l_0(\omega_0 + \omega) \sin \phi \pm 2l_0^2\Omega \sin 2\phi.\end{aligned}\tag{7}$$

Here, each component of $\vec{\Omega} = (\Omega_1, \Omega_2)$ is $\pm(\Omega \sin \phi, \Omega \cos \phi)$ as derived in Appendix A. Eq.(7) indicates D_z and D_y in the coordinate transform from the coordinate system $\{\hat{e}_i\}_{R0}$ into the axis whose unit vectors are aligned with the radius of the curvature and the normal vector against the curvature drawn by the strand. \mathcal{K} is the component of the unit vector that is perpendicular to the radius of the curvature and \hat{e}_3 that is defined for each base pair of the strand. Therefore, the accumulation of \mathcal{K} in Eq.(7) along the strand becomes the kurtosis that makes the curvature of the strand out of the plane to be a superhelix. The important point is how the strand curvature maintains the kurtosis in one direction constantly while the coordinate system $\{\hat{e}_i\}_{R0}$ that is defined for each base pair is rotating 360° in every 10.3 bp. During 10.3 bp turns, the kurtosis involved with ω_0 and the second term in Eq.(7) becomes zero because ϕ is varying from 0° to 360° . In the meantime, $\omega \sin \phi$ has a non negative value during 10.3 bp since ω has the same +/- sign to $\sin \phi$ as shown in Fig. 2B. Maximum value of $r_{11}l_0\omega$ is 0.55 Ang./bp. For 147 bps, \mathcal{K} becomes 8 nm in total. This is slightly extended condition than the diameter of the NP, which is 7 nm. However, the limit of the superhelix that wraps around the NP is no more than this range of kurtosis.

The real kurtosis could vary because of the perturbation of twist deformation from sequence dependent bend twist coupling. However, the condition of \mathcal{K} remains unaltered since the contact angle along the strand should be varied from 0° to 360° in every 10.3 bps, which means the twist(ω) should appear as shown in Fig. 2B in every 10.3 bps. This constant offset from the additional twist (ω) deformation between base pairs makes the strand curvature out of the plane. It completes the superhelix within 1.7 turns that draws the kurtosis with approximately 8 nm.

From the substitution of the angle $\theta=120^\circ$ between two nucleotides in Fig. 1B to $\theta=180^\circ$ makes the slide(D_y) ~ 0 . Therefore, slide(D_y) from $\theta=180^\circ$ that eliminates the major-minor groove in double helix makes the combination $\vec{D}_x + \vec{D}_y$ to be equal to the shift(D_x) and the integration of the kurtosis after the 10.3 bp turn becomes zero. This theoretically driven role of the major-minor groove is validated using simulations using oxDNA whose coarse grained particle is composed of two strands with $\theta = 180^\circ$. The condition of slide(D_y) in oxDNA, which has no major-minor groove difference, causes the increase in the number of wrappings compared

to oxDNA2 with $\theta=120^\circ$ as shown in Fig. 4. More details on the derivation from the absence of the major-minor groove are provided in Appendix F. The results of the details of the simulation are presented in the animated gif files, which are included in the Supplementary video.

4. Discussion

The base pair wise deformation in this paper, which is defined for the localized structure of the strand, seems in juxtaposition against the intrinsic curvature of the strand that has shown a remarkable similarity to the free energy affinity of the nucleosomal DNA[14] or the conformation alike[15]. However, the thermal motion of bending of the strand decides the range of the persistence length, whose coupling with stretch and twist in sequence dependent manner has geometrical constraints. The nonreciprocity of the bend-stretch coupling in Eq. (6) and bend-twist coupling, which is defined in localized deformation in the previous section, enunciates the possible cause of the curvature manifested as persistence length. The base pair wise deformation, therefore, can be regarded as a presumable cause of intrinsic curvature formation, including other various conformations of the double stranded DNA.

Delineating the base-pair wise deformation on the curvature formation process can serve as a beneficial tool for quantifying the localized interaction of the strand with the attachments, the mechanics of curvature formation and the nonlinear dynamics from sequence dependent properties. The charged proteins[6, 7, 8] presumably affect the radius of the base pair cross section and the major-minor groove beyond the restriction presumed in this paper. Yet, elucidating the localized deformation and its propagation along the strand discussed in the paper instigates additional research into the approach for quantifying further intricacy.

The proper quantification of free energy may induce further comprehension of the nucleosomal DNA formation process with the extent to the trajectory from the full assembly of the nucleosomal DNA with histone protein[20] and the helical buckling formation from the classical continuum mechanics in Cosserat theory[36, 37, 38, 39, 40] for a deeper insight to the topological condition[41, 42] induced by $10^2 \sim 10^4$ base pairs in a strand.

To be extended to the emergent dynamics of how wrapping initiates and spreads along the strand, ultimately completing the chromosomes and various curvature forming processes in future research, this onefold derivation has the potential to aid the expression to open out the explicit description for the nonlinear and nonlocal elasticity of the double helix in recent studies[31, 32, 33, 12, 34, 3, 35, 4].

5. Conclusion

In this paper, the geometry of the base pair in the curved strand is measured in 3DNA variables as adjusting Eq.(1)[21] for a set of vectors defined for the nucleotides in the base pair resulting Eq.(4)~Eq.(6). As a result, the geometrically decided twist(ω) deformation derived from roll(ρ) and tilt(τ) in phase characterizes the curvature deformation energetics. The sequence dependent wrapping time and affinity to form a superhelix around the spherical bead affected by the sign of the coupling elasticity $g_{\tau\rho}$ proves that the role of the proper condition between bend and twist deformation during the curvature formation process. Lastly, the kurtosis of the curvature drawn by the strand is derived from the geometrical coupling between translational deformation and rotational deformation. The derivation results in the 1.7 turn of wrapping when the radius of the artificially given core structure is approximately equivalent to that of the nucleosomal DNA.

The conclusions drawn in this research focus entirely on the bare strand's mechanical and geometric characteristics without considering any interactions with proteins or ions. Nonetheless, the result of derivation reveals a geometric restriction that provides insight into the bend-twist coupling condition during curvature formation and highlights the kurtosis that meets the requirement of 1.7 turns.

Acknowledgment

The authors appreciate the fruitful discussion from Prof. Do-Nyun Kim to develop the manuscript. This research is supported by Basic Science Research Program through the National Research Foundation of Korea(NRF) funded by the Ministry of Education (NRF-2020R1I1A1A01071567, NRF-2022R1I1A1A01063582) and National Convergence Research of Scientific Challenges through the National Research Foundation of Korea(NRF) funded by Ministry of Science and ICT (NRF-2020M3F7A1094299). Its computational resources are from National Supercomputing Center with supercomputing resources including technical support (KSC-2020-CRE-0345). There are no conflicts to declare. The code that is used in this paper is available at https://github.com/ieebon/DNA_dynamics.

Appendix A. The geometrical characteristics of the base pair wise deformation

When the cross section of each base pair, \mathcal{A} in the strand is located on the surface of NP with a contact point as shown in Fig. 1, the shortest distance between the center of \mathcal{A} and the central line of the helix Ω^s makes the intersection point on the circumference of \mathcal{A} as marked as a red hollow circle as shown in Fig. 1B. The base pairs in the strand is supposed to have its stacking vector, \vec{l} aligned along the superhelix, Ω^s .

For the verification of Eq.(4)~Eq.(6), the quantified rotation vector $\vec{\Omega}$ in Eq.(1) is essential. When a vector \vec{R} as $\vec{R}_{NP} - \vec{R}_{bp}$ is defined as shown in Fig. 1A, the bending of the strand caused by the curved surface of nanoparticle induces the rotation of the cross section of base pair \mathcal{A} along the direction \hat{e}_3 . More specifically, the cross section \mathcal{A} rotates following the axis that draws a tangent vector on the contact point at the angle ϕ to the surface of NP and the circumference of \mathcal{A} . The norm of the rotation vector component along \hat{e}_1 and \hat{e}_2 becomes equivalent to the inverse of the radius of the curvature, $1/|\vec{R}|$.

The location of the contact with the nanoparticle decides the bending component of the cross section with angle ϕ in Fig. 1B, which is $\pm(-\Omega \cos \phi, \Omega \sin \phi)$. The sign depends on the rotation that the cross section would experience during superhelix formation. Then, the rotational vector of the strand in Eq. (1) is the difference of this vector between cross sections. Therefore, $\vec{\Omega} = \pm(\Omega \sin \phi, \Omega \cos \phi)$. In the main text, the positive sign condition is mainly considered and additionally noted when another case needs to be considered.

Appendix B. Quantification

Full derivation of Eq.(4)~Eq.(6) are as followings:

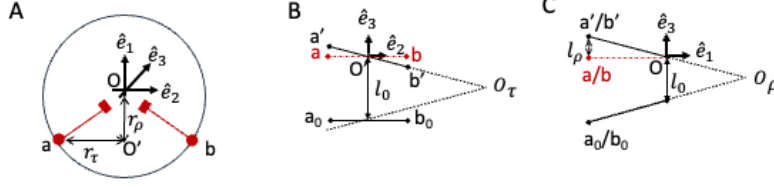


Figure B.6: A. The cross section disk \mathcal{A} with two vectors from the center to two nucleotides a and b . The coordinates of the vectors are $(r_\tau, -r_\rho)$ and $(-r_\tau, -r_\rho)$, respectively. B. A cross section view on $\hat{e}_2 - \hat{e}_3$ plane with the tilt(τ) deformation since the tilt(τ) deformation rotates the base pair along \hat{e}_1 . Two nucleotides on a and b , as shown in A, are supposed to be re-located on a' and b' because of the tilt(τ) deformation. O_τ is the center of the curvature drawn by tilt(τ) deformation, and l_0 is the undeformed stacking distance between base pairs. a_0 and b_0 are the nucleotides in another cross section in the neighbor. C. A cross section view on $\hat{e}_3 - \hat{e}_1$ plane with roll(ρ) deformation. Roll(ρ) deformation rotates the nucleotides along \hat{e}_2 . Therefore, two nucleotides at a and b are to be on a' and b' . O_ρ is the rotation center for the curvature drawn by roll(ρ). a_0 and b_0 are the nucleotides in the cross section in neighbor.

$$\Delta = \Delta_{\hat{e}_1} + \Delta_{\hat{e}_3} = 2r_\tau \frac{d\hat{e}_2}{ds} \cdot l_0 = 2r_\tau l_0 (\Omega_1 \hat{e}_3 - \omega_0 \hat{e}_1). \quad (\text{B.1})$$

$$\Sigma = \Sigma_{\hat{e}_2} + \Sigma_{\hat{e}_3} = -2r_\rho \frac{d\hat{e}_1}{ds} \cdot l_0 = -2r_\rho l_0 (-\Omega_2 \hat{e}_3 + \omega_0 \hat{e}_2). \quad (\text{B.2})$$

$$\Delta l = l_0^2 \frac{d\hat{e}_3}{ds} = l_0^2 (\vec{\Omega} + \omega_0 \hat{e}_3) \times \hat{e}_3 = -l_0^2 (\Omega_1 \hat{e}_2 - \Omega_2 \hat{e}_1). \quad (\text{B.3})$$

Conversion of the deformation in rotational variables like roll(ρ), tilt(τ) and twist(ω) in Eq. (B.1~Eq.(B.3) into curvature unit offers the simple validation of the quantification since the bending component should be equivalent to that of rotational vector $\vec{\Omega}$. The calculation is based on the simple proportionality for the radius of curvature as shown in Fig.B.6. The line from the point that represent the nucleotides a' and b' in Fig. B.6-B and -C to the center of the curvature O_τ and O_ρ is equivalent to the radius of curvature for tilt(τ) and roll(ρ), respectively. The evaluation of each radius of curvature from the proportionality drawn by geometrical condition in the cross section of the base pair \mathcal{A} becomes the followings:

$$\begin{aligned} \overline{a'O'} : \frac{l_\tau}{2} &= \overline{a'O_\tau} : \left(\frac{l_0}{2} + \frac{l_\tau}{2} \right) \\ \overline{a'O_\tau} &= \left(\frac{l_\tau}{2} \right)^{-1} \overline{a'O'} \left(\frac{l_0}{2} + \frac{l_\tau}{2} \right) \end{aligned} \quad (\text{B.4})$$

$$\begin{aligned}\overline{a'O} : l_\rho &= \overline{a'O_\rho} : \left(\frac{l_0}{2} + l_\rho \right) \\ \overline{a'O_\rho} &= (l_\rho)^{-1} \overline{a'O} \left(\frac{l_0}{2} + l_\rho \right)\end{aligned}\quad (\text{B.5})$$

r_τ and r_ρ in Fig. B.6.A is the distance between the nucleotide and O' along $\hat{\mathbf{e}}_1$ and $\hat{\mathbf{e}}_2$, respectively. The proportionality of r_τ and r_ρ to $\overline{a'O_\tau}$ and $\overline{a'O_\rho}$ calculates the deformation caused by roll(ρ) and tilt(τ) in curvature unit[nm^{-1}].

Appendix C. Energetics

The energy of the deformation of the strand in curvature is known to be as followings[1, 43]:

$$\beta E_{MS} = \frac{1}{2} \int_0^L ds (A_1 \Omega_\tau^2 + A_2 \Omega_\rho^2 + C \Omega_\omega^2 - 2G_1 \Omega_\rho \Omega_\omega + 2M_{12} \Omega_\tau \Omega_\rho + 2M_{13} \Omega_\tau \Omega_\omega). \quad (\text{C.1})$$

Here, the set of elastic moduli is $(A_1, A_2, C, G_1, M_{12}, M_{13}) = [63.0, 38.8, 53.2, 102.0, 0.4, 0.4][nm]$ from oxDNA2 simulation by averaging the sequence dependent elasticity[43].

Unlike the energy contribution, the most minor coupling force is important to acquire the necessary resolution for proceeding the deformation process accordingly. The most negligible coupling forces involved in the curvature formation of superhelix are $F_{\tau-\rho}$ and $F_{\omega-\tau}$ in $O(10^{-2})$ in pN which to form the coupling curvature between tilt and roll($\tau - \rho$) and that of twist and roll($\omega - \tau$). The perturbation of the system, like random noise exceeding more than $O(10^{-2})$, will disturb the forming process of the curvature. For this subtlety, the simulation conducted with the conventional Langevin thermostat has an unwrapping process numerous times so that the new thermostat based on the heat diffusion process is adapted.

Appendix D. Simulation details

Potential energy function between NP and oxDNA particle is defined with Lennard-Johns's potential energy function extended with minimum cutoff distance. It is nearly identical to the diameter of the nanoparticle to fix the boundary of the nanoparticle, which is defined as a point mass with +64 C with a mass of 26700 in the unit of oxDNA, which is 5.24×10^{-25} kg. This is the same mass of nano particles composed of 64 gold atoms. The potential energy modeling is inspired by the DNA ratchet system suggested by Park et al.[44]. The Coulomb force between a nanoparticle and a nucleotide is modeled with exponential function with relaxation parameter. Two types of potential energy are adapted for the interaction between the strand and the NP. LJ expanded potential energy function that expresses the expulsion force between two objects is as below:

$$E_{LJ} = -4\epsilon \left[\left(\frac{\sigma}{r - \Delta} \right)^6 - \left(\frac{\sigma}{r - \Delta} \right)^{12} \right], r < r_c + \Delta \quad (\text{D.1})$$

C/AGT/C	C/AAT/C	$g_{\rho\omega}$		$g_{\tau\omega}$		$g_{\tau\rho}$	
		IAT	EXAT	IAT	EXAT	IAT	EXAT
CA	CA	106.2	106.2	1.9	1.9	0.56	0.56
AG	AA	104.0	100.2	-1.0	1.52	-0.3	0.51
GT	AT	105.6	95.09	1.6	-0.91	-0.6	-0.58
TC	TC	103.3	103.3	-1.76	-1.76	1.03	1.03

Table E.1: Coupling rigidity differences at replaced sequence in IAT and EXAT.

r is the variable that represents the distance between particles in the oxDNA strand and NP. The parameters are $\epsilon = 23.52pNm$, $\sigma = 0.48nm$, $\Delta = 4.0nm$ and $r_c = 0.68nm$. For Coulomb force, the Debye potential energy function is used as follows:

$$E = C \frac{q_i q_j}{\epsilon r} \exp(-\kappa r), r < r_c \quad (D.2)$$

The parameters are $\epsilon = 1$, $\kappa = 2.97nm$, $r_c = 4.26nm$, $q_i = -0.2e$ and $q_j = 64e$.

New thermostat that is included in the simulation is explained in Supplementary material. The code information is in Acknowledgement. Note that the subtlety of the force acting on the bend twist coupling, which is derived from Eq. (C.1) allows extremely fine resolution of forces applied on each particle during simulation. The conventionally used damping parameter in the Langevin thermostat provides the random force that countermands the coupling force in range of $O(10^{-2})$ in pN . For the wrapping process, damping coefficient η should be given as $> 10^5$ [ps] for the random force defined as $\sqrt{k_B T m} / (\eta \cdot dt)$ [pN] = $1.5e2 \sqrt{(1/\eta)}$ [pN] for oxDNA2 package in LAMMPS.

Appendix E. Sequences in strands

From the sequence information of all five strands that are adapted in the simulation, which are c1/c2/c3 and IAT/EXAT, the replacement of the partial sequence in the strand is supposed to cause the difference of wrapping affinity and speed. The cause of such difference is highlighted with the coupling rigidity between tilt(τ) and roll(ρ), $g_{\tau\rho}$. For each replacement, two neighbors of that sequence also have the alternation of the rigidity. For example, when AGT is replaced with AAT surrounded by cytosins, 4 pairs of sequences are replaced as shown in Table 1. Fortunately, all replacements have the same sequences for their neighbors during four replacement times for each type of coupling rigidity against the sequence in IAT and EXAT in Table 1. Unlike $g_{\rho\omega}$ and $g_{\tau\omega}$, which has very few differences in the range of the rigidity value, $g_{\tau\rho}$ has a different number in positive sign. Such a trend is more drastically given for c1/c2/c3 strands. From the c2 strand, the c1 strand has eight TA replacements with all different neighbor sequences. c3 strand has five TAs among those. All the coupling rigidity, including its neighbors, are marked in table S3~S11 in Supplementary material. The total number of the positive $g_{\rho\tau}$ in the replaced sequences is counted in Fig. E.7 with the affinity of wrapping conformation for each strand. c1 has 20 $g_{\rho\tau}$ cases out of 24 sequence pair points that is affected by the replacement. c2 and c3 strands less number of $g_{\rho\tau} > 0$ compared to c1 strand. The affinity of wrapping conformation and rapid wrapping speed of the c1 strand bolsters the importance of $g_{\rho\tau} > 0$.

/

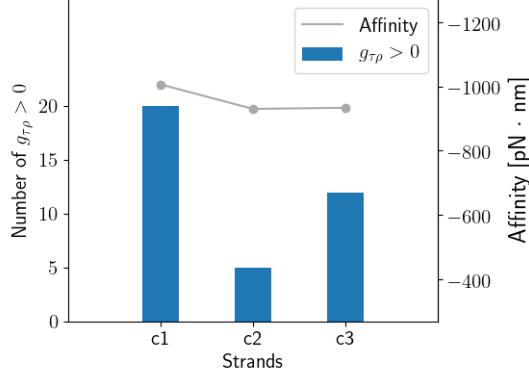


Figure E.7: Count of $g_{\tau\rho} > 0$ sequences and affinity for c1, c2 and c3 strand.

Appendix F. Mm groove for 1.7 turn

When there is no difference between major and minor grooves, the angle between two nucleotides can be presumed to be 180 degrees. In this condition, the coordinates of vector and which are pointing from the center of the base pair to each nucleotide. The result with the angle $\theta = 180^\circ$ between two nucleotides located at $\vec{r}_1 = (-r_{nt}, 0)$ $\vec{r}_2 = (r_{nt}, 0)$ in Eq. (4) and Eq.(5) are as followings:

$$1/2\Delta = -\left(\frac{d\vec{r}_1}{ds} - \frac{d\vec{r}_2}{ds}\right) = 2r_{nt}(\Omega_1\hat{e}_3 - \omega_0\hat{e}_1), \quad (\text{F.1})$$

$$1/2\Sigma = \left(\frac{d\vec{r}_1}{ds} - \frac{d\vec{r}_2}{ds}\right) = 0 \quad (\text{F.2})$$

Since there is no Σ in Eq.(7), the kurtosis from the strand with no major-minor groove becomes zero. Therefore, the wrapping number around NP using oxDNA depends on the repulsion between coarse-grained particles in the oxDNA model. One of the differences we can confirm through oxDNA1 and oxDNA2 with heat diffusion damping term or Langevin thermostat in the confirmation set up in Fig. 5 is the wrapping number of the strand. For the simulation, 375 bp ds strand with AT(red) and CG(gray) combination is conducted with one end fixed. The movie for each case is added as Supplementary Video SV2 and SV3 for oxDNA1 and oxDNA2, respectively.

The derivation of kurtosis from Eq. (4)~Eq.(6) is straightforward with coordinate transformation matrix, Φ as followings:

$$\begin{bmatrix} \hat{e}_R \\ \hat{e}_K \end{bmatrix} = \Phi \begin{bmatrix} \hat{e}_\epsilon \\ \hat{e}_\infty \end{bmatrix} = \begin{bmatrix} \cos\phi' & -\sin\phi' \\ \sin\phi' & \cos\phi' \end{bmatrix} \begin{bmatrix} \hat{e}_2 \\ \hat{e}_1 \end{bmatrix} \quad (\text{F.3})$$

here, $\hat{\mathbf{e}}_{\mathcal{R}}$ $\hat{\mathbf{e}}_{\mathcal{K}}$ are the coordinate system defined along $\vec{R} = \vec{R}_{NP} - \vec{R}_{bp}$ and the axis along kurtosis, which is the orthogonal vector defined between $\hat{\mathbf{e}}_{\mathcal{R}}$ and $\hat{\mathbf{e}}_3$. $\phi' = 180 - \phi$. For the kurtosis, we have $\hat{\mathbf{e}}_{\mathcal{K}} = -\sin\phi\hat{\mathbf{e}}_2 + \cos\phi\hat{\mathbf{e}}_1$.

References

- [1] E. Skoruppa, E. Carlon, Equilibrium fluctuations of dna plectonemes, *Phys. Rev. E* 106 (2022). URL: <GotoISI>://WOS:000860422300006<https://journals.aps.org/pre/pdf/10.1103/PhysRevE.106.024412>.
- [2] A. Marin-Gonzalez, J. G. Vilhena, F. Moreno-Herrero, R. Perez, Dna crookedness regulates dna mechanical properties at short length scales, *Phys. Rev. Lett.* 122 (2019) 48102. URL: <https://www.ncbi.nlm.nih.gov/pubmed/30768347>. doi:10.1103/PhysRevLett.122.048102.
- [3] E. Skoruppa, A. Voorspoels, J. Vreede, E. Carlon, Length-scale-dependent elasticity in dna from coarse-grained and all-atom models, *Phys. Rev. E* 103 (2021). URL: <GotoISI>://WOS:000650949800008<https://journals.aps.org/pre/pdf/10.1103/PhysRevE.103.042408>.
- [4] K. Liebl, M. Zacharias, Accurate modeling of dna conformational flexibility by a multivariate ising model, *Proc. Natl. Acad. Sci.* 118 (2021). URL: <https://www.ncbi.nlm.nih.gov/pubmed/33876759>.
- [5] J. Yoo, S. Park, C. Maffeo, T. Ha, A. Aksimentiev, Dna sequence and methylation prescribe the inside-out conformational dynamics and bending energetics of dna minicircles, *Nucleic Acids Res.* 49 (2021) 11459–11475. URL: <https://www.ncbi.nlm.nih.gov/pubmed/34718725>. doi:10.1093/nar/gkab967.
- [6] C. Tan, T. Terakawa, S. Takada, Dynamic coupling among protein binding, sliding, and dna bending revealed by molecular dynamics, *J. Am. Chem. Soc.* 138 (2016) 8512–8522. URL: <https://www.ncbi.nlm.nih.gov/pubmed/27309278>. doi:10.1021/jacs.6b03729.
- [7] C. Tan, S. Takada, Dynamic and structural modeling of the specificity in protein-dna interactions guided by binding assay and structure data, *J Chem Theory Comput* 14 (2018) 3877–3889. URL: <https://www.ncbi.nlm.nih.gov/pubmed/29806939>. doi:10.1021/acs.jctc.8b00299.
- [8] K. Kamagata, E. Mano, K. Ouchi, S. Kanbayashi, R. C. Johnson, High free-energy barrier of 1d diffusion along dna by architectural dna-binding proteins, *J. Mol. Biol.* 430 (2018) 655–667. URL: <https://www.ncbi.nlm.nih.gov/pubmed/29307468>. doi:10.1016/j.jmb.2018.01.001.
- [9] R. M. Harrison, F. Romano, T. E. Ouldrige, A. A. Louis, J. P. Doye, Identifying physical causes of apparent enhanced cyclization of short dna molecules with a coarse-grained model, *Journal of Chemical Theory and Computation* 15 (2019) 4660–4672. doi:10.1021/acs.jctc.9b00112.
- [10] A. Vologodskii, M. D. Frank-Kamenetskii, Strong bending of the dna double helix, *Nucleic Acids Research* 41 (2013) 6785–6792. doi:10.1093/nar/gkt396.
- [11] J. Shin, O. C. Lee, W. Sung, How a short double-stranded dna bends, *J. Chem. Phys.* 142 (2015) 155101. URL: <https://www.ncbi.nlm.nih.gov/pubmed/25903911>. doi:10.1063/1.4916379.
- [12] M. Kim, S. Bae, I. Oh, J. Yoo, J. S. Kim, Sequence-dependent twist-bend coupling in dna minicircles, *Nanoscale* 13 (2021) 20186–20196. URL: <https://www.ncbi.nlm.nih.gov/pubmed/34847218>. doi:10.1039/d1nr04672a.
- [13] M. Caraglio, E. Skoruppa, E. Carlon, Overtwisting induces polygonal shapes in bent DNA, *The Journal of Chemical Physics* 150 (2019) 135101. URL: <https://doi.org/10.1063/1.5084950>. doi:10.1063/1.5084950. [arXiv:https://pubs.aip.org/aip/jcp/article-pdf/doi/10.1063/1.5084950/15558694/135101.1.online.pdf](https://pubs.aip.org/aip/jcp/article-pdf/doi/10.1063/1.5084950/15558694/135101.1.online.pdf).
- [14] G. S. Freeman, J. P. Lequieu, D. M. Hinckley, J. K. Whitmer, J. J. de Pablo, Dna shape dominates sequence affinity in nucleosome formation, *Phys. Rev. Lett.* 113 (2014) 168101. URL: <https://www.ncbi.nlm.nih.gov/pubmed/25361282>. doi:10.1103/PhysRevLett.113.168101.
- [15] S. Bae, I. Oh, J. Yoo, J. S. Kim, Effect of dna flexibility on complex formation of a cationic nanoparticle with double-stranded dna, *ACS Omega* 6 (2021) 18728–18736. URL: <https://www.ncbi.nlm.nih.gov/pubmed/34337212>.
- [16] J. A. Nash, A. Singh, N. K. Li, Y. G. Yingling, Characterization of nucleic acid compaction with histone-mimic nanoparticles through all-atom molecular dynamics, *ACS Nano* 9 (2015) 12374–12382. URL: <https://doi.org/10.1021/acs.nano.5b05684>. doi:10.1021/acs.nano.5b05684.
- [17] A. A. Travers, G. Muskhelishvili, J. M. Thompson, Dna information: from digital code to analogue structure, *Philos. Trans. R. Soc. A* 370 (2012) 2960–2986. URL: <https://www.ncbi.nlm.nih.gov/pubmed/22615471>. doi:10.1098/rsta.2011.0231.
- [18] T. J. Richmond, C. A. Davey, The structure of dna in the nucleosome core, *Nature* 432 (2003).
- [19] A. Garai, S. Saurabh, Y. Lansac, P. K. Maiti, Dna elasticity from short dna to nucleosomal dna, *J. Phys. Chem. B* 119 (2015) 11146–11156. URL: <https://www.ncbi.nlm.nih.gov/pubmed/26134918>. doi:10.1021/acs.jpcb.5b03006.
- [20] G. B. Brandani, C. Tan, S. Takada, The kinetic landscape of nucleosome assembly: A coarse-grained molecular dynamics study, *PLoS Comput Biol* 17 (2021) e1009253. URL: <https://www.ncbi.nlm.nih.gov/pubmed/34314440>. doi:10.1371/journal.pcbi.1009253.
- [21] J. F. Marko, E. D. Siggia, Bending and twisting elasticity of dna, *Macromolecules* 27 (1994) 981–988. doi:10.1021/ma00082a015.

- [22] S. K. Nomidis, M. Caraglio, M. Laleman, K. Phillips, E. Skoruppa, E. Carlon, Twist-bend coupling, twist waves, and the shape of dna loops, *Phys. Rev. E* 100 (2019) 22402. URL: <https://www.ncbi.nlm.nih.gov/pubmed/31574750>. doi:10.1103/PhysRevE.100.022402.
- [23] X. J. Lu, W. K. Olson, 3dna: a versatile, integrated software system for the analysis, rebuilding and visualization of three-dimensional nucleic-acid structures, *Nat. Protoc.* 3 (2008) 1213–1227. URL: <https://www.ncbi.nlm.nih.gov/pubmed/18600227>. doi:10.1038/nprot.2008.104.
- [24] S. Li, W. K. Olson, X. J. Lu, Web 3dna 2.0 for the analysis, visualization, and modeling of 3d nucleic acid structures, *Nucleic Acids Res.* 47 (2019) W26–W34. URL: <https://www.ncbi.nlm.nih.gov/pubmed/31114927>. doi:10.1093/nar/gkz394.
- [25] J. M. Carnerero, S. Masuoka, H. Baba, Y. Yoshikawa, R. Prado-Gotor, K. Yoshikawa, Decorating a single giant dna with gold nanoparticles, *RSC Adv* 8 (2018) 26571–26579. URL: <https://www.ncbi.nlm.nih.gov/pubmed/35541036>. doi:10.1039/c8ra05088k.
- [26] A. Diaz, B. Y. Gu, Y. Li, S. J. Plimpton, D. L. McDowell, Y. P. Chen, A parallel algorithm for the concurrent atomistic-continuum methodology, *J. Comput. Phys.* 463 (2022). URL: <GotoISI>://WOS:000806760800005.
- [27] H. Koh, S. Chiashi, J. Shiomi, S. Maruyama, Heat diffusion-related damping process in a highly precise coarse-grained model for nonlinear motion of swcnt, *Sci. Rep.* 11 (2021). URL: <GotoISI>://WOS:000621919500026.
- [28] G. B. Brandani, T. Niina, C. Tan, S. Takada, Dna sliding in nucleosomes via twist defect propagation revealed by molecular simulations, *Nucleic Acids Res.* 46 (2018) 2788–2801. URL: <https://www.ncbi.nlm.nih.gov/pubmed/29506273>. doi:10.1093/nar/gky158.
- [29] M. Watanabe, W. P. Reinhardt, Direct dynamical calculation of entropy and free energy by adiabatic switching, *Phys. Rev. Lett.* 65 (1990) 3301–3304. URL: <https://www.ncbi.nlm.nih.gov/pubmed/10042834>. doi:10.1103/PhysRevLett.65.3301.
- [30] D. Frenkel, B. Smit, Understanding molecular simulation: from algorithms to applications, Elsevier, 2023.
- [31] K. Chakraborty, M. Kang, S. M. Loverde, Molecular mechanism for the role of the h2a and h2b histone tails in nucleosome repositioning, *J. Phys. Chem. B* 122 (2018) 11827–11840. URL: <https://www.ncbi.nlm.nih.gov/pubmed/30477297>. doi:10.1021/acs.jpcc.8b07881.
- [32] A. Marin-Gonzalez, J. G. Vilhena, R. Perez, F. Moreno-Herrero, A molecular view of dna flexibility, *Q. Rev. Biophys.* 54 (2021) e8. URL: <https://www.ncbi.nlm.nih.gov/pubmed/34225835>. doi:10.1017/S0033583521000068.
- [33] M. Zoli, Twisting and bending stress in dna minicircles, *Soft Matter* 10 (2014) 4304–4311. URL: <https://www.ncbi.nlm.nih.gov/pubmed/24791278>. doi:10.1039/c3sm52953c.
- [34] E. Skoruppa, S. K. Nomidis, J. F. Marko, E. Carlon, Bend-induced twist waves and the structure of nucleosomal dna, *Phys. Rev. Lett.* 121 (2018) 88101. URL: <https://www.ncbi.nlm.nih.gov/pubmed/30192578>. doi:10.1103/PhysRevLett.121.088101.
- [35] S. K. Nomidis, E. Skoruppa, E. Carlon, J. F. Marko, Twist-bend coupling and the statistical mechanics of the twistable wormlike-chain model of dna: Perturbation theory and beyond, *Phys. Rev. E* 99 (2019) 32414. URL: <https://www.ncbi.nlm.nih.gov/pubmed/30999490>. doi:10.1103/PhysRevE.99.032414.
- [36] M. Gazzola, L. H. Dudte, A. G. McCormick, L. Mahadevan, Forward and inverse problems in the mechanics of soft filaments, *R. Soc. Open. Sci.* 5 (2018) 171628. URL: <https://www.ncbi.nlm.nih.gov/pubmed/30110439>. doi:10.1098/rsos.171628.
- [37] S. Neukirch, Writhing instabilities of twisted rods: from infinite to finite length, *J. Mech. Phys. Solids* 50 (2002) 1175–1191. doi:10.1016/s0022-5096(01)00130-2.
- [38] J. M. T. Thompson, G. H. M. van der Heijden, S. Neukirch, Supercoiling of dna plasmids: mechanics of the generalized ply, *Proc. R. Soc. A* 458 (2002) 959–985. doi:10.1098/rspa.2001.0901.
- [39] G. H. M. van der Heijden, S. Neukirch, V. G. A. Goss, J. M. T. Thompson, Instability and self-contact phenomena in the writhing of clamped rods, *Int. J. Mech. Sci.* 45 (2003) 161–196. doi:10.1016/s0020-7403(02)00183-2.
- [40] J. M. T. Thompson, Cutting dna: Mechanics of the topoisomerase, *Eur. Phys. J.* 165 (2008) 175–182. URL: <GotoISI>://WOS:000261698100019. doi:10.1140/epjst/e2008-00861-1.
- [41] B. D. Coleman, W. K. Olson, D. Swigon, Theory of sequence-dependent dna elasticity, *The Journal of Chemical Physics* 118 (2003) 7127–7140. URL: <https://doi.org/10.1063/1.1559690>. doi:10.1063/1.1559690. arXiv:https://pubs.aip.org/aip/jcp/article-pdf/118/15/7127/19192815/7127_1_online.pdf.
- [42] M. Zuiddam, R. Everaers, H. Schiessel, Physics behind the mechanical nucleosome positioning code, *Phys. Rev. E* 96 (2017) 052412. URL: <https://link.aps.org/doi/10.1103/PhysRevE.96.052412>. doi:10.1103/PhysRevE.96.052412.
- [43] E. Skoruppa, M. Laleman, S. K. Nomidis, E. Carlon, Dna elasticity from coarse-grained simulations: The effect of groove asymmetry, *J. Chem. Phys.* 146 (2017) 214902. URL: <https://www.ncbi.nlm.nih.gov/pubmed/28595422>. doi:10.1063/1.4984039.
- [44] S. Park, J. Song, J. S. Kim, In silico construction of a flexibility-based dna brownian ratchet for directional nanoparticle delivery, *Sci. Adv.* 5 (2019). URL: <GotoISI>://WOS:000466398400062.